Nuclear Instruments and Methods in Physics Research B 343 (2015) 83–88

Contents lists available at ScienceDirect

Nuclear Instruments and Methods in Physics Research B

journal homepage: www.elsevier.com/locate/nimb

Nonuniform plasma diffusion and multi-pulse effect in plasma-based ion implantation

B.C. Zheng, M.K. Lei *

Surface Engineering Laboratory, School of Materials Science and Engineering, Dalian University of Technology, Dalian 116024, China

ARTICLE INFO

Article history:
Received 25 September 2014
Received in revised form 6 November 2014
Accepted 7 November 2014

Keywords:
Plasma-based ion implantation (PBII)
Fluid model
Plasma diffusion
Multi-pulse

ABSTRACT

The nonuniform plasma caused by plasma diffusion and the incomplete plasma recovery during short pulse-off time have great influences on the sheath dynamics and the implantation efficiency in plasma-based ion implantation (PBII). In this paper, a magnetized plasma diffusion fluid model is established to describe the plasma diffusion in PBII process. Together with a magnetized sheath fluid model, the full pulse period including sheath dynamics during pulse-on time and plasma recovery during pulse-off time can be described, and the models are verified to be accurate by comparing with experimentally measured electron density profiles. The influence of process parameters on sheath dynamics, the influence of incomplete plasma recovery under multi-pulse bias on implantation efficiency are investigated by solving the presented models with considering plasma diffusion. It is found that the variations of process parameters which accelerate the plasma diffusion reduce the steady-state sheath thickness and increase the ion implantation current, and vice versa. Change the pulse frequency from 1 kHz to 100 kHz under typical PBII process parameters significantly increases the average ion implantation current density, and the limiting factor which affects the implantation efficiency is converted from duty cycle to plasma diffusion. Increasing the plasma density and decreasing the transverse magnetic field are the effective methods to improve the implantation efficiency as well. The results reported here help to provide a theoretical guidance for the parameters optimization in PBII process.

1. Introduction

Plasma-based ion implantation (PBII) is an effective surface modification technique developed by Conrad in 1987 [1], which can eliminate the line-of-sight restriction of conventional ion beam implantation and has been demonstrated to be very effective in improving the wear and corrosion resistance for metals and alloys [2,3]. Since the ion acceleration occurs mainly in the sheath during PBII process, the sheath dynamics is extremely important and has been investigated by analytical theories and computer simulations in the past [4–6]. In addition, to suppress secondary electrons emission [7], enhance ion implantation uniformity and increase plasma density [8], an external magnetic field can be introduced into PBII and the process has been studied experimentally [9] and numerically [10,11].

In these pioneering researches, a uniform plasma distribution is normally assumed during the simulation, although in practice the plasma around the target is expected to be nonuniform due to plasma diffusion [12,13]. In addition, these aforementioned researches only considered a single pulse, under the assumption that plasma has enough time between pulses to flow back into the sheath region, where the ions are drained and implanted into the target during pulse-on time. However, the off time between pulses is generally not long enough for complete plasma recovery, especially for the magnetized plasma. For the components with irregular shape, such as inner surface of tube [14] or PBII batching [15], the sheath overlap caused by incomplete plasma recovery could result in the depletion of ion implantation dose and the deterioration of modification uniformity. Moreover, the recovery process determined by plasma diffusion is influenced by process parameters, and appropriate pulse parameters such as pulse length and duty cycle should be adopted under different process parameters. Some numerical studies using particle-in-cell (PIC) method [16,17] and fluid model [18] have demonstrated that the plasma dynamics parameters, such as sheath expansion and ion implantation current must be affected during the next pulse-on time if the plasma recovers incompletely. Chung et al. [19] experimentally investigated the plasma recovery during pulse-off time in PBII and compared the results with a fluid model [20]. However, the primary reason for plasma recovery, namely the plasma diffusion is ignored in their model. Moreover, these existing models for

* Corresponding author. Tel.: +86 411 84707255; fax: +86 411 84706192.
E-mail address: surfeng@dlut.edu.cn (M.K. Lei).

http://dx.doi.org/10.1016/j.nimb.2014.11.025
0168-583X/

plasma recovery were studied in the absence of magnetic field, and no systematic studies have been reported about the effects of plasma diffusion and multi-pulse bias in PBII.

In this paper, a magnetized plasma diffusion fluid model is built up using the equations of ion continuity and ion motion, and adopting a variable diffusion coefficient of the ion. The validity of the presented models is identified by comparing with measured electron density profiles. The influences of plasma diffusion and incomplete plasma recovery under multi-pulse bias in PBII are studied using the presented models. The results reported here help to provide a theoretical guidance for the parameters optimization in PBII process.

2. Magnetized plasma diffusion fluid model

2.1. Model description

Under the low working pressure in PBII, the ions collide with neutrals at an effective ion velocity $|\boldsymbol{u}_i|$, namely the ion drift velocity rather than the ion thermal velocity u_{th}. The ion mobility μ_i depends on the ion drift velocity $|\boldsymbol{u}_i|$ and can be written as [21]:

$$\mu_i = \frac{2q\lambda_i}{\pi M|\boldsymbol{u}_i|} \tag{1}$$

where q is the ion charge, $\lambda_i = 1/(n_g\sigma_m)$ is the ion mean-free path, n_g is the neutral gas density, σ_m is the ion-neutral momentum transfer cross-section, and M is the mass of the ion. Under a magnetic field, the mobility of ions traversed the magnetic field can be derived as [21]:

$$\mu_{\perp i} = \frac{\mu_i}{1+(\omega_c\tau_m)^2} \tag{2}$$

where $\omega_c = qB/M$ is the ion rotation frequency, B is the magnetic field strength, $\tau_m = 1/\nu_m$, $\nu_m = |\boldsymbol{u}_i|/\lambda_i$ is the ion-neutral momentum transfer frequency. For the plasma diffusion perpendicular to the magnetic field, adopting an experimentally verified diffusion coefficient $D_{\perp a} \approx \mu_{\perp i}T_e$ [22], which can be written as:

$$D_{\perp a} \approx \mu_{\perp i}T_e = \frac{2qT_e\lambda_i}{\pi M}\frac{|\boldsymbol{u}_i|}{|\boldsymbol{u}_i|^2+(\omega_c\lambda_i)^2} \tag{3}$$

where T_e is the electron temperature in V, and the corresponding electric field is [22]:

$$\boldsymbol{E} = -T_e\frac{\nabla n_i}{n_i} \tag{4}$$

where n_i is the ion density. Substituting the ion flux $\Gamma = -D_{\perp a}\nabla n_i$ into the ion continuity equation:

$$\frac{\partial n_i}{\partial t} + \nabla\cdot(\Gamma) = K_{iz}n_gn_e \tag{5}$$

then (5) becomes:

$$\frac{\partial n_i}{\partial t} - \frac{2qT_e\lambda_i}{\pi M}\nabla\cdot\left(\frac{|\boldsymbol{u}_i|}{|\boldsymbol{u}_i|^2+(\omega_c\lambda_i)^2}\nabla n_i\right) = K_{iz}n_gn_e \tag{6}$$

where t is time, K_{iz} is the ionization rate coefficient of electron-neutral collision and $n_e = n_i$ is the electron density. Together with the ion motion equation:

$$\frac{\partial \boldsymbol{u}_i}{\partial t} = -\boldsymbol{u}_i\cdot\nabla\boldsymbol{u}_i + \frac{q}{M}(\boldsymbol{E}+\boldsymbol{u}_i\times\boldsymbol{B}) - \frac{qT_i}{M}\frac{\nabla n_i}{n_i} - \frac{F_c}{M} \tag{7}$$

where T_i is the ion temperature, and F_c is the collisional drag force, which can be written as [23]:

$$F_c = \frac{\pi}{2}Mv_m\boldsymbol{u}_i \tag{8}$$

and substituting (4) and (8) into the ion motion (7) then:

$$\frac{\partial \boldsymbol{u}_i}{\partial t} = -\boldsymbol{u}_i\cdot\nabla\boldsymbol{u}_i - \frac{q(T_e+T_i)}{M}\frac{\nabla n_i}{n_i} + \frac{q}{M}\boldsymbol{u}_i\times\boldsymbol{B} - \frac{\pi}{2}v_m\boldsymbol{u}_i \tag{9}$$

During pulse-off time, the electrons flood back into the sheath region on a time scale of about the inverse electron plasma frequency and neutralize the net charge in this region, therefore the electric field is vanished and the ions in the sheath are not further accelerated toward the target. When all the energetic ions reach the target surface, a floating sheath will be formed on it. The electric force dominates the magnetic Lorentz force as one approaching the plasma boundary [24], therefore the ion flux near the target surface can be written as $\Gamma = -D_a\nabla n_i$, where $D_a \approx \mu_i T_e$ is the plasma ambipolar diffusion coefficient in the absence of magnetic field. Ignoring the floating sheath thickness, the ion velocity on the target surface is the Bohm velocity:

$$u_B = -D_a\frac{\nabla n_i}{n_i}\bigg|_{\text{target}} \tag{10}$$

then the boundary condition of ion density on the target surface can be derived from (10) as:

$$\nabla n_i|_{\text{target}} = -\frac{\pi}{2}\frac{n_i}{\lambda_i} \tag{11}$$

Therefore, the initial nonuniform plasma before applying the negative pulsed bias onto the target and the plasma recovery during pulse-off time can be described by solving the nonlinear Eqs. (6) and (9):

$$\begin{aligned}&\frac{\partial n_i}{\partial t} - \frac{2qT_e\lambda_i}{\pi M}\nabla\cdot\left(\frac{|\boldsymbol{u}_i|}{|\boldsymbol{u}_i|^2+(\omega_c\lambda_i)^2}\nabla n_i\right) = K_{iz}n_gn_e\\ &\frac{\partial \boldsymbol{u}_i}{\partial t} = -\boldsymbol{u}_i\cdot\nabla\boldsymbol{u}_i - \frac{q(T_e+T_i)}{M}\frac{\nabla n_i}{n_i} + \frac{q}{M}\boldsymbol{u}_i\times\boldsymbol{B} - \frac{\pi}{2}v_m\boldsymbol{u}_i\end{aligned} \tag{12}$$

with the boundary condition of Eq. (11). For describing the plasma diffusion outside the sheath region during pulse-on time, the boundary condition on the sheath boundary is:

$$\nabla n_i|_{\text{sb}} = -\frac{\pi}{2}\frac{n_i}{\lambda_i} \tag{13}$$

and the sheath boundary is defined where the ion velocity is the Bohm velocity u_B.

However, the Eq. (12) are not appropriate to describe the sheath dynamics and the ion implantation process in the sheath region during pulse-on time, for which a well-established sheath fluid model is used, which composed of the equations of ion continuity and ion motion, Poisson's equation, and Boltzmann's relationship of electrons,

$$\begin{aligned}&\frac{\partial n_i}{\partial t} + \nabla\cdot(n_i\boldsymbol{u}_i) = 0\\ &\frac{\partial \boldsymbol{u}_i}{\partial t} + (\boldsymbol{u}_i\cdot\nabla)\boldsymbol{u}_i = \frac{q}{M}(-\nabla\varphi + \boldsymbol{u}_i\times\boldsymbol{B}) - \frac{\pi}{2}v_m\boldsymbol{u}_i\\ &\nabla^2\varphi = -\frac{q}{\varepsilon_0}\left(n_i - n_0\exp\left(\frac{\varphi}{T_e}\right)\right)\end{aligned} \tag{14}$$

where φ is the plasma potential, ε_0 is the permittivity of free space. The boundary condition for Eq. (14) is:

$$\varphi|_{\text{target}} = \varphi_p \tag{15}$$

where φ_p is the negative bias on the target.

In summary, the full pulse period including the sheath dynamics during pulse-on time and the plasma recovery during pulse-off time can be modeled and calculated repeatedly by these models. The initial nonuniform plasma before applying the negative pulsed bias onto the target, the plasma diffusion outside the sheath region during pulse-on time and the plasma recovery during pulse-off time can be described by solving the Eq. (12) with the boundary condition of Eqs. (11) or (13). The sheath dynamics and the ion implantation process in the sheath region during pulse-on time

are described by solving the Eq. (14) with the boundary condition of Eq. (15). The influences of plasma diffusion and multi-pulse bias in PBII are studied by adopting the presented models in Section 3.

2.2. Model validation

The diffusion coefficient perpendicular to the magnetic field used in the magnetized plasma diffusion fluid model are in good agreement with experimental diagnosis for a range of magnetic fields and gas pressures [22]. Without the magnetic field, the models degrade to the plasma low-pressure nonsteady diffusion fluid model [18], which has been verified to be accurate comparing with the PIC method [16]. Here, in order to identify the validity of the presented models, the experimental results of electron density profiles by Chung et al. [19] are selected as a comparison.

Fig. 1(a) shows the temporal variations of electron density profiles with the distance from target under various times measured by Chung et al. [19], converted from the measured electron saturation current at various probe positions. The absolute electron density has not been given directly, but can be derived as about 6×10^{14} ions/m^3 at the position 13 cm away from the target, according to the sheath position at the end of pulse-on time under the negative bias of −3.3 kV. The electron temperature T_e is 4.2 V and the diagnosis range is up to $l_0 = 13$ cm from the target. The working gas is Ar under pressure of 5×10^{-2} Pa, whose ion-neutral momentum transfer cross-section can be approximately assumed as $\sigma_m = 2 \times 10^{-18}$ m^{-2} under ion temperature of 0.026 V [25]. The ionization rate coefficient of e-Ar collision can be calculated by numerical integration [21]:

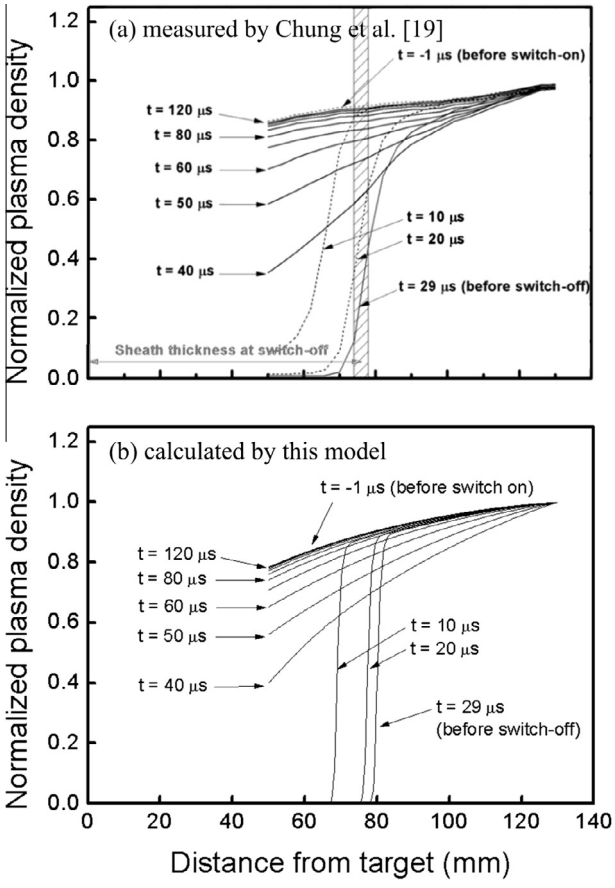

Fig. 1. Temporal variations of electron density profiles with the distance from target under various times (a) measured by Chung et al. [19] and (b) calculated by this model.

$$K_{iz}(T_e) = \langle v\sigma_{iz}(v)\rangle = \left(\frac{m}{2\pi e T_e}\right)^{3/2} \int_0^\infty 4\pi v^3 \sigma_{iz}(v) \exp\left(-\frac{mv^2}{2eT_e}\right) dv \quad (16)$$

where v is the electron velocity, σ_{iz} is the electron impact ionization cross section, m is the electron mass, e is the elementary charge. In order to improve the numerical convergence, the computed ionization rate coefficient is fitted to Arrhenius form:

$$K_{iz}(\Theta_e) = 2.3 \times 10^{-14} \Theta_e^{0.59} \exp(17.44/\Theta_e)\ \mathrm{m}^3/\mathrm{s} \quad (17)$$

where $\Theta_e = T_e/T_0$ is the normalized electron temperature and $T_0 = 1$ V is the unit electron temperature.

From Fig. 1(a) it can be seen that before the bias is applied, the plasma diffuses from the bulk plasma to the target and achieves a nonuniform density distribution. During pulse-on time, a plasma sheath is formed on the target surface, and expands towards the bulk plasma. During pulse-off time, the depleted region is gradually recovered due to the ambipolar diffusion from the bulk plasma, the recovery speed is decelerated with time and the plasma is not completely recovered even after 90 μs pulse-off time.

In order to verify the modeling results with the experimental diagnosis, considering a one dimensional planar coordinate with a target at $x = 0$ and a bulk plasma at $x = l_0$, and assuming the plasma can be provided with density $n_0 = 6 \times 10^{14}$ ions/m^3 continuously by the bulk plasma. The boundary condition is:

$$n_i|_{x=l_0} = n_0 \quad (18)$$

With aforementioned boundary condition, the models are solved to describe the initial nonuniform plasma, the sheath dynamics during 30 μs pulse-on time and the plasma recovery during 90 μs pulse-off time. For 1-D planar geometry, the magnetized plasma diffusion fluid model and the magnetized sheath fluid model can be represented as:

$$\begin{aligned}
\frac{\partial n_i}{\partial t} &= \frac{2qT_e\lambda_i}{\pi M}\frac{\partial}{\partial x}\left(\frac{|\boldsymbol{u}_i|}{|\boldsymbol{u}_i|^2 + (\omega_c\lambda_i)^2}\frac{dn_i}{dx}\right) + K_{iz}n_g n_e \\
\frac{\partial u_x}{\partial t} &= -u_x\frac{\partial u_x}{\partial x} - \frac{q(T_e+T_i)}{Mn_i}\frac{dn_i}{dx} + \frac{q}{M}u_y B - \frac{\pi}{2}\frac{1}{\lambda_i}|\boldsymbol{u}_i|u_x \\
\frac{\partial u_y}{\partial t} &= -u_x\frac{\partial u_y}{\partial x} - \frac{q}{M}u_x B - \frac{\pi}{2}\frac{1}{\lambda_i}|\boldsymbol{u}_i|u_y
\end{aligned} \quad (19)$$

$$\begin{aligned}
&\frac{\partial n_i}{\partial t} + \frac{\partial}{\partial x}(n_i u_x) = 0 \\
&\frac{\partial u_x}{\partial t} + u_x\frac{\partial u_x}{\partial x} = \frac{q}{M}\left(-\frac{\partial\varphi}{\partial x} + u_y B\right) - \frac{\pi}{2}\frac{|\boldsymbol{u}_i|}{\lambda_i}u_x \\
&\frac{\partial u_y}{\partial t} + u_x\frac{\partial u_y}{\partial x} = -\frac{q}{M}u_x B - \frac{\pi}{2}\frac{|\boldsymbol{u}_i|}{\lambda_i}u_y \\
&\frac{\partial^2\varphi}{\partial x^2} = -\frac{q}{\varepsilon_0}\left(n_i - n_0\exp\left(\frac{\varphi}{T_e}\right)\right)
\end{aligned} \quad (20)$$

where u_x and u_y are the component of $\boldsymbol{u}_i$ at x and y directions, respectively, B is the transverse magnetic field along z direction. The Eqs. (19) and (20) are first normalized and discretized, and solved using finite difference method. The nonlinear Poisson's equation in Eq. (20) is solved by linearization and iteration, until the process converges [4].

Fig. 1(b) shows the electron density profiles calculated by these models, under the same process conditions as Fig. 1(a). During the calculation, the space and time steps are taken as 0.025 cm and 0.05 ns, respectively, and the initial nonuniform plasma is assumed to be steady when the change of normalized ion density in 1 μs is less than 10^{-4}. From the comparison in Fig. 1 it can be seen that all the initial nonuniform plasma, the sheath dynamics during pulse-on time and the plasma recovery during pulse-off time are well

reproduced, implies that the presented models have incorporated all the primary processes correctly and are acceptable to describe the plasma diffusion in PBII.

3. Results and discussion

3.1. Influence of nonuniform plasma diffusion in PBII

In PBII process, applying a negative pulsed bias on the target leads to an ion matrix sheath formation which gradually expands to the steady-state Child-law sheath. Under the assumption of uniform plasma distribution and given process parameters, the steady-state sheath thickness s can be obtained conveniently from the Child-law current density [21]:

$$J = \frac{4}{9}\varepsilon_0\left(\frac{2e}{M}\right)^{1/2}\frac{\varphi_p^{3/2}}{s^2} \tag{21}$$

and the ion current density near the sheath boundary $J = en_0u_B$. However, the plasma density is nonuniform outside the sheath due to plasma diffusion and decreases from the bulk plasma to the target, and the steady-state sheath thickness cannot be determined directly from the aforementioned method.

Here, the models established in Section 2 are adopted to investigate the influence of plasma diffusion on sheath expansion and ion implantation process in PBII. During calculation, the following typical PBII process parameters are applied: the bulk plasma density n_0 is 1×10^{16} ions/m^3, the distance between bulk plasma and target l_0 is 0.1 m, the working pressure p is 5×10^{-2} Pa, the transverse magnetic field B is 0 G, the electron temperature T_e is 2 V, and the negative pulsed bias φ_p is -10 kV. Under multi-pulse condition, the typical pulse frequency f is 100 kHz. The working gas is N_2 and the ion is assumed as N_2^+, with an ion-neutral momentum transfer cross-section of about $\sigma_m = 2 \times 10^{-18}$ m^{-2} under ion temperature of 0.026 V [25], and the ionization rate coefficient of e-N_2 collision is [26]:

$$K_{iz}(\Theta_e) = 1.95 \times 10^{-15}\Theta_e^{1.13}\exp(-14.4/\Theta_e)\ \mathrm{m}^3/\mathrm{s} \tag{22}$$

Fig. 2 gives the relationship of steady-state sheath position with corresponding ion implantation current density under typical PBII process parameters with and without considering plasma diffusion, and changes some process parameters in the typical range of PBII separately. Three curves represent the Child-law current density under typical PBII process parameters with three different voltages of -2, -5 and -10 kV, the horizontal dashed line is the ion implantation current density given by $J = en_0u_B$. Without considering plasma diffusion, a uniform plasma with density n_0 is assumed between the bulk plasma and the target, and the steady-state sheath thickness can be predicted from the intersections of $J = en_0u_B$ and the Child-law curves under different biases. The ion current density of about 4.2 A/m^2 under typical PBII process parameters and the corresponding sheath thicknesses of 0.016, 0.03 and 0.048 m calculated by the magnetized sheath fluid model without considering plasma diffusion are represented by 'o' points and are consistent with the intersections predicted above.

However, in order to coincide with the actual PBII process, the plasma diffusion is considered by solving the presented models and the results are shown in Fig. 2. Under the typical PBII process parameters, the lower than n_0 plasma density near the sheath boundary results in a widened steady-state sheath thickness of about 0.06 m and a reduced ion implantation current density of about 2.8 A/m^2, compared with uniform plasma assumption without considering plasma diffusion. In addition, increasing the bulk plasma density n_0 from 1 to 2×10^{16} ions/m^3, the sheath thickness reduces and ion implantation current density increases, which is natural due to the plasma density near the sheath boundary is increased. Reducing the negative pulsed bias φ_p from -10 to -5 kV, both the steady-state sheath thickness and ion implantation current density decrease due to the lower plasma density near sheath boundary under thinner sheath thickness, which is consistent with experiment results [12]. Under given bulk plasma density and negative pulsed bias, the steady-state sheath thickness and the corresponding ion implantation current density are influenced by electron temperature and transverse magnetic field as well, due to the diffusion ability of plasma is changed. For example, under a transverse magnetic field B of 400 G, the weakened plasma diffusion results in an increased steady-state sheath thickness, which has the identical trend with experimental diagnosis [27].

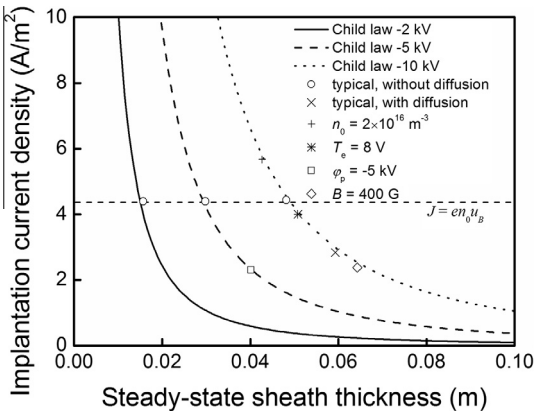

Fig. 2. Relationship of steady-state sheath thickness with ion implantation current density, (o): under typical PBII process parameters of $l_0 = 0.1$ m, $n_0 = 1 \times 10^{16}$ ions/m^3, $p = 5 \times 10^{-2}$ Pa, $B = 0$ G, $T_e = 2$ V, $\varphi_p = -10$ kV without considering plasma diffusion, and (x): considering plasma diffusion, and changing the process parameters separately as (+): $n_0 = 2 \times 10^{16}$ ions/m^3, (*): $T_e = 8$ V, (□):$\varphi_p = -5$ kV, (◇): $B = 400$ G.

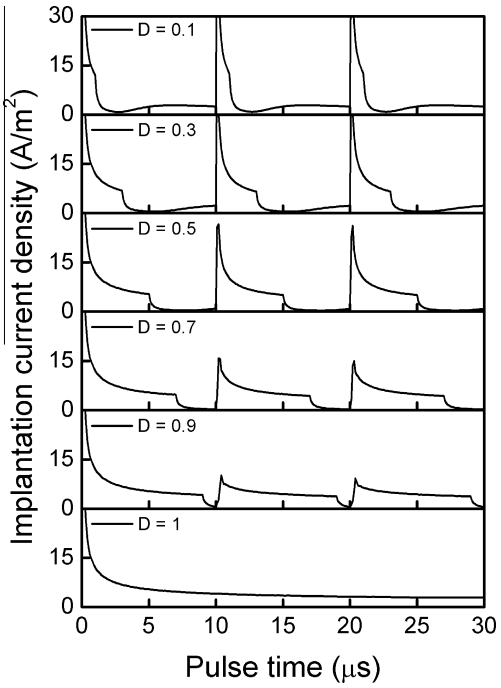

Fig. 3. Time dependence of ion implantation current density during three pulses under typical PBII process parameters of $n_0 = 1 \times 10^{16}$ ions/m^3, $l_0 = 0.1$ m, $p = 5 \times 10^{-2}$ Pa, $B = 0$ G, $T_e = 2$ V, $\varphi_p = -10$ kV, and $f = 100$ kHz, considering plasma diffusion and changing the duty cycle D from 0.1 to 1.

3.2. Influence of multi-pulse effect in PBII

The incomplete plasma recovery under multi-pulse bias has great influence in PBII process. Fig. 3 shows the time dependence of ion implantation current density during three pulses under the typical PBII process parameters of $n_0 = 1 \times 10^{16}$ ions/m^3, $l_0 = 0.1$ m, $p = 5 \times 10^{-2}$ Pa, $B = 0$ G, $T_e = 2$ V, $\varphi_p = -10$ kV, and $f = 100$ kHz, considering plasma diffusion and changing the duty cycle D from 0.1 to 1. The peaks appeared at the beginning of each pulse correspond to the evacuation of ion matrix sheath, and gradually decrease to the space-charge limited flow. During pulse-off time, the current densities are dramatically reduced due to the sheath has been flooded by the electrons and as a consequence the ions are not further accelerated towards the target. Under low duty cycles such as 0.1 and 0.3, the plasma recovers nearly completely during pulse-off time and there are no significant difference between the first and the latter two pulses. However, under higher duty cycles, both the peak and average ion implantation current densities decrease during the latter two pulses, due to the incomplete plasma recovery diminishes the plasma supply during the next pulse-on time. In that case, the implantation process during each pulse tends to achieve a periodic equilibrium state, which means that the plasma depletion during pulse-on time is recovered during the next pulse-off time, and the plasma distribution at the beginning of the latter pulse is same as the former one. The necessary time to achieve this periodic equilibrium state is several pulses under typical PBII process parameters and can be ignored comparing with the actual processing time. Therefore, this equilibrium state under multi-pulse bias should be considered as more reasonable in practice, rather than the single pulse case.

In order to investigate the influence of process parameters on the implantation efficiency under multi-pulse bias, Fig. 4 shows the dependence of average ion implantation current density with duty cycle under typical PBII process parameters of $n_0 = 1 \times 10^{16}$ ions/m^3, $l_0 = 0.1$ m, $p = 5 \times 10^{-2}$ Pa, $B = 0$ G, $T_e = 2$ V, $\varphi_p = -10$ kV, and $f = 100$ kHz, considering plasma diffusion and changing the parameters separately as $f = 1$ kHz, $n_0 = 2 \times 10^{16}$ ions/m^3, $T_e = 8$ V, $\varphi_p = -5$ kV, and $B = 400$ G, the results are obtained under the periodic equilibrium state mentioned above. Decreasing the pulse frequency from 100 to 1 kHz, the average ion implantation current density decreases significantly. The variation with increasing the duty cycle converts from a first increase then decrease to a linear increase, and under both of the pulse frequencies the average ion implantation current density converges to about 2.8 A/m^2 as the duty cycle closing to 1. The reason is, under the lower pulse frequency of 1 kHz therefore a longer pulse period, the ion implantation current density is in the space-charge limited flow of 2.8 A/m^2 during most of the pulse-on time, and the average ion implantation current density increases linearly with the duty cycle. However, under the higher pulse frequency of 100 kHz there is a large proportion of peak current in the pulse-on time, the steep plasma density gradient during pulse-off time accelerates the plasma diffusion and increases the average ion implantation current density beyond the space-charge limited flow of 2.8 A/m^2 to about 4.1–4.2 A/m^2 under the duty cycle of 0.5–0.9. The implantation efficiency under lower pulse frequency of 1 kHz is limited by duty cycle while under higher pulse frequency of 100 kHz is limited by plasma diffusion. An optimum exists in the regulating range of duty cycle under higher pulse frequency of 100 kHz. The results are similar with the calculated results by PIC method [17], which possess an increased current density as increasing the pulse frequency as well. However, a fixed ion current density is set as the calculation boundary [17] and therefore is the maximum current density under duty cycle of 1. By increasing the bulk plasma density n_0 from 1 to 2×10^{16} ions/m^3, the implantation efficiency increases linearly as expected. The increase of electron temperature T_e from 2 to 8 V enhances the plasma diffusion and therefore improves the implantation efficiency. Lowering the negative pulsed bias φ_p from −10 to −5 kV, the sheath thickness is narrowed and the plasma diffusion during pulse-off time is weakened, which reduces the implantation efficiency. Increasing the magnetic field B from 0 to 400 G, the plasma diffusion is decreased significantly and can be ignored during pulse-off time, the average ion implantation current density increases with increasing the duty cycle and the implantation efficiency is limited by duty cycle. Selecting appropriate duty cycle under high pulse frequency can avoid both the low implantation efficiency under short pulse-on time and the nonuniform modification under long pulse-on time. In addition, increasing the plasma density without overheating the processed component and decreasing the transverse magnetic field as much as possible are the effective methods to improve the implantation efficiency.

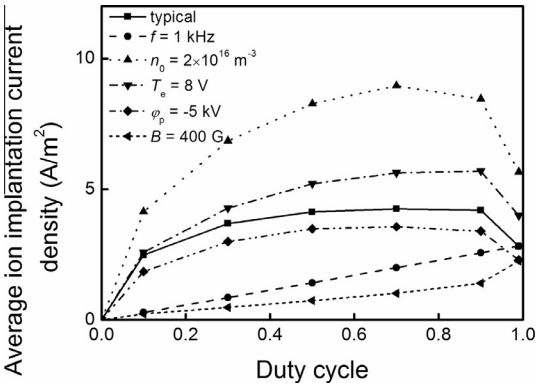

Fig. 4. Dependence of average ion implantation current density with duty cycle under typical PBII process parameters of $n_0 = 1 \times 10^{16}$ ions/m^3, $l_0 = 0.1$ m, $p = 5 \times 10^{-2}$ Pa, $B = 0$ G, $T_e = 2$ V, $\varphi_p = -10$ kV, and $f = 100$ kHz, considering plasma diffusion and changing the process parameters separately as $f = 1$ kHz, $n_0 = 2 \times 10^{16}$ ions/m^3, $T_e = 8$ V, $\varphi_p = -5$ kV, $B = 400$ G.

4. Conclusions

(1) A magnetized plasma diffusion fluid model is built up using the equations of ion continuity and ion motion, and a variable diffusion coefficient of the ion. Together with a magnetized sheath fluid model, the full pulse period including sheath dynamics during pulse-on time and plasma recovery during pulse-off time can be described, and the models are verified to be accurate by comparing with experimental diagnosis.

(2) The nonuniform plasma caused by plasma diffusion has great influences in PBII process and should be considered. For example, under typical PBII process parameters, by considering plasma diffusion the steady-state sheath thickness increases from 0.05 to 0.06 m and the corresponding ion implantation current density decreases from about 4.2–2.8 A/m^2. The variations of process parameters which accelerate the plasma diffusion reduce the steady-state sheath thickness and increase the ion implantation current, and vice versa.

(3) Increasing the pulse frequency from 1 to 100 kHz under typical PBII process parameters significantly increases the average ion implantation current density, and the limiting factor which affects the implantation efficiency is converted from duty cycle to plasma diffusion. The implantation efficiency increases linearly with the bulk plasma density and decreases significantly under the transverse magnetic field, while other process parameters have no such significant impact.

Acknowledgements

The Authors would like to appreciate Dr. Y. Li and Mr. Z.Y. Wang for the contributory discussions. This work is supported by the National Science Foundation of China under Grants Nos. 50725519, 51271048 and 51321004.

References

[1] J.R. Conrad, J. Appl. Phys. 62 (1987) 777.
[2] M.K. Lei, Y.X. Ou, K.S. Wang, L. Chen, Surf. Coat. Technol. 205 (2011) 4602.
[3] S. Mandl, C. Diaz, J.W. Gerlach, J.A. Garcia, Nucl. Instrum. Methods B 307 (2013) 305.
[4] G.A. Emmert, M.A. Henry, J. Appl. Phys. 71 (1992) 113.
[5] X.B. Tian, P.K. Chu, Phys. Lett. A 277 (2000) 42.
[6] Y.H. Li, X.C. Li, Y.N. Wang, Surf. Coat. Technol. 229 (2013) 168.
[7] M. Ueda, I.H. Tan, R.S. Dallaqua, J.O. Rossi, Surf. Coat. Technol. 201 (2007) 6597.
[8] D.L. Tang, R.K.Y. Fu, X.B. Tian, P. Peng, P.K. Chu, Nucl. Instrum. Methods B 206 (2003) 808.
[9] E. Pillaca, M. Ueda, H. Reuther, C.M. Lepienski, Surf. Coat. Technol. 246 (2014) 1.
[10] K.G. Kostov, M.A. Algatti, E.J.D.M. Pillaca, M.E. Kayama, R.P. Mota, R.Y. Honda, Eur. Phys. J. D 54 (2009) 205.
[11] N.N. Safa, H. Ghomi, M. Khoramabadi, S. Ghasemi, A.R. Niknam, Vacuum 101 (2014) 354.
[12] M. Keidar, O.R. Monteiro, I.G. Brown, Appl. Phys. Lett. 76 (2000) 3002.
[13] Y.X. Huang, X.B. Tian, S.Q. Yang, R.K.Y. Fu, P.K. Chu, Surf. Coat. Technol. 201 (2007) 5458.
[14] B. Liu, C.Z. Liu, D.J. Cheng, G.L. Zhang, R. He, S.Z. Yang, Nucl. Instrum. Methods B 184 (2001) 644.
[15] Y. Lu, L.P. Wang, X.F. Wang, IEEE Trans. Plasma Sci. 41 (2013) 1644.
[16] B.P. Wood, J. Appl. Phys. 73 (1993) 4770.
[17] B. Briehl, H.M. Urbassek, J. Phys. D Appl. Phys. 35 (2002) 462.
[18] Y. Li, B.C. Zheng, M.K. Lei, IEEE Trans. Plasma Sci. 41 (2013) 43.
[19] K.J. Chung, B. Jung, J.M. Choe, G.H. Kim, Y.S. Hwang, Thin Solid Films 547 (2013) 13.
[20] K.J. Chung, J.M. Choe, G.H. Kim, Y.S. Hwang, Thin Solid Films 521 (2012) 197.
[21] M.A. Lieberman, A.J. Lichtenberg, Principles of Plasma Discharges and Materials Processing, John Wiley & Sons Inc., New Jersey, 2005.
[22] F. Vidal, T.W. Johnston, J. Margot, M. Chaker, O. Pauna, IEEE Trans. Plasma Sci. 27 (1999) 727.
[23] T.E. Sheridan, M.J. Goeckner, J. Appl. Phys. 77 (1995) 4967.
[24] J.E. Allen, Phys. Plasmas 14 (2007) 024701.
[25] A.V. Phelps, J. Phys. Chem. Ref. Data 20 (1991) 557.
[26] K. Tao, D. Mao, J. Hopwood, J. Appl. Phys. 91 (2002) 4040.
[27] M. Keidar, O.R. Monteiro, A. Anders, I.D. Boyd, Appl. Phys. Lett. 81 (2002) 1183.